g FACTORS IN ^{116,118,120}Sn: SENSITIVITY TO CONFIGURATIONS NEAR THE FERMI SURFACE

M. C. East[1], A. E. Stuchbery[1], A. N. Wilson[1,2], P. M. Davidson[1], T. Kibedi[1], A. I. Levon[3]

[1]*Department of Nuclear Physics, Research School of Physical Sciences and Engineering, The Australian National University, Canberra, Australia*
[2]*Department of Physics, The Australian National University, Canberra, Australia*
[3]*Institute for Nuclear Research, National Academy of Sciences of Ukraine, Kyiv, Ukraine*

The transient-field technique has been used to measure the $g(2_1^+)$ values in 116,118,120Sn, simultaneously, relative to each other and to the well-known $g(2_1^+)$ values in the stable even Pd isotopes. The *g* factor in ^{118}Sn, which has a small positive value, evidently differs from those in 116Sn and $^{120–124}$Sn, which have small negative values. This behavior is investigated through shell model calculations. The experimental *g* factors are also compared with recent QRPA and RQRPA calculations.

The Sn isotopes, with magic proton number $Z = 50$, have been of enduring experimental and theoretical interest; see, for example [1 - 9] and references therein. The recent development of radioactive ion beams has enabled the study of Sn isotopes between the double shell closures at neutron-deficient $^{100}_{50}Sn_{50}$ and neutron-rich $^{132}_{50}Sn_{82}$. Very recently, B(E2) data on neutron-deficient isotopes have shown an enhancement over the simplest shell model predictions [7 - 9]. The data, together with large-basis shell model calculations [7, 8], imply contributions in the 2_1^+ states of 2*p*-2*h* and 4*p*-4*h* proton excitations across the $Z = 50$ shell gap and/or neutron core excitations across the $N = 50$ shell gap. Measurements of the *g* factors could test this interpretation and discriminate between the contributions from proton and neutron configurations. Before measurements on radioactive Sn isotopes are undertaken, however, it is important to revisit the *g*-factor measurements on the stable isotopes (^{112}Sn-^{124}Sn).

The *g* factors of the 2_1^+ states in the stable even Sn isotopes were measured by Hass et al. [3] in 1980 using the transientfield technique with NaI detectors and a sequence of different separated-isotope targets. The data suggest that $g(2_1^+)$ in ^{118}Sn is near zero, perhaps with a positive sign, whereas the $g(2_1^+)$ values in the neighboring isotopes ^{116}Sn and ^{120}Sn are negative. This previous work is limited somewhat by the calibration of the transientfield strength relative to the Cd isotopes (each with an uncertainty of ~ 30 %).

We report here new measurements of the *g* factors in ^{116,118,120}Sn relative to each other and relative to the *g* factors of the stable even Pd isotopes, which have uncertainties of the order of 5 % [10]. The aims of the present experiment are to (i) focus on ^{118}Sn and examine the suggestion that its $g(2_1^+)$ value is more positive than those of the neighboring isotopes, and (ii) constrain the scale of the absolute *g* factors in the stable Sn isotopes by a simultaneous transient-field measurement relative to the stable Pd isotopes. A new measurement of the absolute magnitude of the *g* factors was considered important in view of recent calculations in a relativistic quasiparticle random phase approximation (RQRPA) model [11], which predict positive *g* factor values between ~ +0.2 and ~ +0.1 for ^{114}Sn through ^{124}Sn, in clear conflict with the existing data, which however might be considered uncertain due to the normalization procedure employed.

Experiments were performed using the ANU 14UD Pelletron accelerator. The target consisted of an annealed iron foil 4.70 mg/cm^2 thick onto which were evaporated contiguous layers of natural Sn and Pd, 0.73 and 0.06 mg/cm^2 thick, respectively. The Pd layer (melting point 1552 °C) on the front surface of the target served to (i) prevent the loss of the Sn layer (melting point 232 °C) under beam bombardment and (ii), provide an absolute calibration of the transient-field strength so that absolute *g* factors can be obtained by reference to independent, previous measurements. The iron foil was backed by an evaporated layer of indium 2.07 mg/cm^2 thick and then was pressed on to a copper foil, nominally 12.5 μm thick, which had also been annealed under vacuum. In contrast with the usual target fabrication procedure, the evaporation of a thick layer of copper on the back of the iron foil was avoided due to the risk of destroying the previously evaporated layer of Sn, given its low melting point. To help offset the adverse effects of beam heating, the target was held near 5 K throughout the experiment, by mounting it on the second stage of a cryocooler (Sumitomo RDK-408D) with a cooling capacity of 1 W at 4 K. A beam of ^{58}Ni at energy of 190 MeV was made incident upon the ^{nat}Pd face of the target. The beam intensity was maintained at approximately 3 pnA. No deterioration of the target due to the intense beam was evident.

Backscattered ^{58}Ni ions were detected in two rectangular silicon photodiode detectors 9.2 mm wide by 10.13 mm high positioned symmetrically above and below the beam axis in a plane 16.2 mm from the target. The separation between the two particle detectors was 7.75 mm. The signals from these two detectors were processed separately but the symmetry of the angular correlations allowed the data for the individual particle detectors to be added together during the analysis. Gamma rays were detected in coincidence with backscattered Ni ions. Two pairs of Ge γ -ray detectors were placed at $\theta\gamma = \pm 65°$ and $\theta\gamma = \pm 115°$ relative to the incident beam direction. The target-to-detector distance was chosen so that the faces of the Ge crystals subtend an angle of 36◦ with respect to the beam spot on the target. An external polarizing field of 0.08 T was applied to the target. The direction of the field was reversed every ~ 15 minutes to minimize systematic errors.

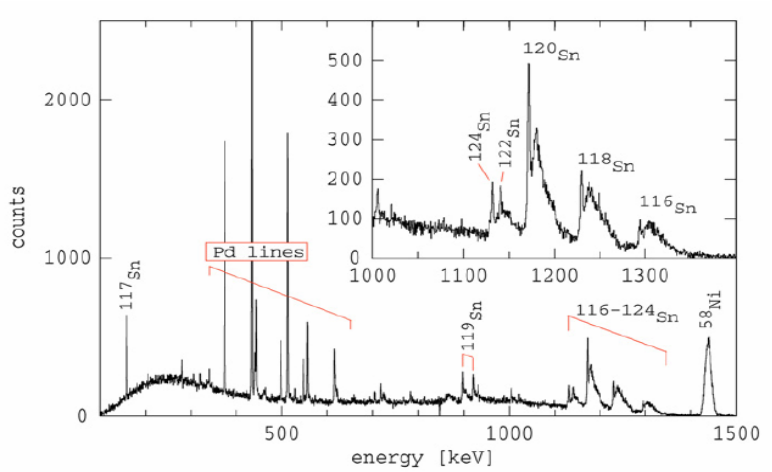

Fig. 1. Gamma-ray spectrum for the detector at +65° to the beam. 'Field up' and 'field down' spectra have been added together. Note that many of the excited Sn nuclei decay in flight, as evidenced by the Doppler-broadened high-energy tails of the Sn peaks.

Fig. 1 shows an example of a random-subtracted γ-ray spectrum for the detector at +65° to the beam. Peak integration and background subtraction was straightforward for the Pd lines of interest. It was more complicated for the Sn peaks due to their Doppler broadened line shapes. Whereas the peaks for ^{116}Sn, ^{118}Sn and ^{120}Sn remain well separated, it was not possible to separate the Doppler broadened lines from ^{122}Sn and ^{124}Sn.

Experimental g factors were obtained by the transient-field method, following standard procedures [12 - 17]. Table 1 outlines the calculated reaction kinematics for the Sn and Pd isotopes of interest. Although the transient-field strength was calibrated using the measured precessions and known g factors of the stable Pd isotopes, Table 1 shows calculations of the transient field using the parametrization $B_{TF} = 21.5 \cdot Z \cdot (v/v_0)^{0.41}$ Tesla, which has been shown to be valid for ^{46}Pd [12] and ^{52}Te [17] ions under similar kinematic conditions. These calculations of the transient-field precession were used only to scale the strength of the transient field between the several isotopes studied; i.e., (i) to account for the small differences due to the Z dependence of the transient field, (ii) to scale for the slight variations in the reaction kinematics and energy loss for the various isotopes, and (iii) to scale the magnitude of the net precession due to differences in the nuclear lifetimes. The extracted g factors are not sensitive to reasonable choices of transient-field parametrization for these scaling procedures. For example, negligible differences result if the Rutgers parametrization [18] is used for the scaling instead.

Table 1. **Kinematics for Pd and Sn recoiling in iron. $\tau(2_1^+)$ is the mean life of the 2_1^+ level. (E_i) and (E_e) are the average energies with which the ions enter into and exit from the iron foil. The corresponding ion velocities are (v_i/v_0) and (v_e/v_0), where $v_0 = c/137$ is the Bohr velocity. The average ion velocity is (v/v_0). The time for ions to traverse the iron layer is t_{Fe}. φ is the transient-field precession per unit g factor, calculated as described in the text. These quantities were calculated with the stopping powers of Ziegler et al. [19]**

Isotope	$\tau(2_1^+)$ (ps)	$\langle E_i \rangle$ (MeV)	$\langle E_e \rangle$ (MeV)	$\langle v_i/v_0 \rangle$	$\langle v_e/v_0 \rangle$	$\langle v/v_0 \rangle$	t_{Fe} (fs)	$-\phi(\tau)$ (mrad)
^{104}Pd	14.3	150.8	16.6	7.65	2.53	4.61	583	51.1
^{106}Pd	17.5	149.8	16.2	7.55	2.48	4.58	590	51.5
^{108}Pd	34.5	148.8	15.9	7.45	2.43	4.54	601	52.2
^{110}Pd	67.1	147.8	15.6	7.36	2.39	4.51	608	52.7
^{116}Sn	0.54	144.2	14.4	7.07	2.23	4.88	331	29.6
^{118}Sn	0.70	143.2	14.0	7.00	2.18	4.74	380	33.6
^{120}Sn	0.92	142.3	13.8	6.91	2.15	4.62	429	37.5

The experimental precession angle is given by $\Delta\Theta = \varepsilon / S$, where S is the logarithmic derivative of the angular correlation at the γ -ray detection angle [12 - 17]. The 'effect', ε, was evaluated as usual from double ratios of counts recorded for field 'up' and field 'down' in the pairs of detectors at ±65° and ±115°. Formally, $\varepsilon = (N\downarrow - N\uparrow)/(N\downarrow + N\uparrow)$, where N is the number of counts detected at angle $+\theta$ and ↑ and ↓ denote the direction of the magnetic field.

The angular correlations, and hence S, were calculated, for both the Sn and Pd isotopes, as described in Ref. [17], utilizing the theory of Coulomb excitation. S values are effectively identical for the Sn isotopes, but vary across the Pd isotopes due to the effect of feeding from higher excited states. Matrix elements for the Coulomb excitation calculations were obtained from the literature [20, 21], which includes experimental B(E2) values and electric quadrupole moment measurements. The calculations for the Sn isotopes included the first excited state only as the probability of multiple

excitations is negligible. For the Pd isotopes, however, it was necessary to include the 0_2^+, 2_2^+ and 4_1^+ excited states. The population of these states affects the precession measurement chiefly through their decays into the 2_1^+ state, which reduce the net alignment. This feeding intensity increases across the Pd isotopes, from ^{104}Pd to ^{110}Pd, and is manifest in the reduction of *S* values for increasing mass in the Pd isotopes seen in Table 2. The reliability of the calculated angular correlations for this type of measurement has been confirmed by numerous measurements and calculations (see Ref. [17] for more extensive references).

Table 2. **Summary of measured precession angles in the even Pd and Sn isotopes. $\epsilon(\pm 65^\circ)$ and $\epsilon(\pm 115^\circ)$ are the measured "effect" for the detector pairs at ±65° and ±115°, respectively. The "slope" parameters *S*(65°) and *S*(115°) are calculated as described in the text**

Isotope	E_γ (keV)	$\epsilon(\pm 65°)$ ($\times 10^3$)	$S(65°)$	$\epsilon(\pm 115°)$ ($\times 10^3$)	$S(115°)$	$\langle \Delta\Theta \rangle$ (mrad)	present	g_{2^+} previous	adopted
^{104}Pd	556	38(21)	−2.53	−69(26)	2.52	−22(5)		+0.415(25)[a]	
^{106}Pd	512	33(10)	−2.29	−51(12)	2.27	−21(3)		+0.400(20)[a]	
^{108}Pd	434	42(8)	−2.03	−44(9)	2.02	−18(3)		+0.353(17)[a]	
^{110}Pd	374	24(11)	−1.75	−55(12)	1.74	−20(6)		+0.335(15)[a]	
^{116}Sn	1293	−19(28)	−2.97	−2(46)	2.96	+4.5(80)	−0.15(26)	−0.16(10)[b]	−0.16(9)
^{118}Sn	1229	18(15)	−2.97	−18(15)	2.96	−5.9(36)	+0.17(10)	+0.02(10)[b]	+0.10(7)
^{120}Sn	1171	−4(12)	−2.97	16(11)	2.96	+3.5(27)	−0.09(7)	−0.14(7)[b]	−0.12(5)

[a] Weighted average of previous measurements; see Ref. [10].
[b] Ref. [3].

In the present work the main uncertainty in the calculation of the angular correlations for the Pd isotopes stems from uncertainties in the intensities of the transitions that feed from the 0_2^+, 2_2^+ and 4_1^+ states into the 2_1^+ state. These intensities, however, were determined from experiment with ample precision for the present purpose. The experimental feeding intensities were also found to agree well with intensities deduced from Coulomb excitation cross-sections calculated using matrix elements from the literature. Feeding corrections have a negligible impact on the uncertainty in the average value of $\langle \Delta\theta/\mathrm{g} \rangle = -54 \pm 5$ mrad for the Pd isotopes, which was used to normalize the Sn *g*-factor measurements.

The results of the present measurement of the *g* factors in ^{116}Sn, ^{118}Sn and ^{120}Sn, normalized to the Pd isotopes, are summarized in Table 2 and compared with the previous results [3]. There are several important differences between the present and previous work which underscore the reliability of the present approach: First, our measurements on the Sn and Pd isotopes were performed simultaneously, relative to each other, using high-resolution HPGe γ-ray detectors, whereas the previous work used a sequence of targets and much poorer resolution NaI detectors. Simultaneous measurements such as those performed here eliminate virtually all sources of systematic error in this type of measurement. Secondly, the present measurement relative to the well-known *g* factors of the Pd isotopes provides a more reliable measure of the absolute magnitude of the *g* factors than did the previous calibration relative to the Cd isotopes.

Despite the differences in the experimental approach, the present and previous works are in good agreement. Having established the reliability of the previous work, in the following discussion a weighted average of the present and previous results is adopted for the $g(2_1^+)$ values in ^{116}Sn, ^{118}Sn and ^{120}Sn. The overlapping peaks for ^{122}Sn and ^{124}Sn, which were not separable in the γ-ray spectra, yield a combined *g* factor of -0.27(15), reasonably consistent the previously reported values for ^{122}Sn and ^{124}Sn of -0.07(11) and -0.15(10), respectively. The present measurement adds weight to the hint in previous data that ^{118}Sn has a positive *g* factor whereas the neighboring isotopes, ^{116}Sn and ^{120}Sn have negative *g* factors. In fact the average experimental *g* factor (combining present and previous work) for ^{116}Sn and $^{120-124}$Sn is -0.13(4). Thus the difference between $g(2_1^+)$ in ^{118}Sn and this average value for the neighboring isotopes is +0.23(8) – a difference of almost 3 standard deviations.

The following discussion will first focus on the *g* factor of ^{118}Sn, seeking to understand how it could have a small positive value when its neighbors have negative *g* factors. We will then take a more global approach to discuss the overall magnitude of the experimental *g* factors across the range of Sn isotopes in comparison with theory, particularly the recent QRPA [6] and RQRPA [11] calculations.

1. A positive *g* factor in ^{118}Sn

We now seek to understand how the *g* factor in ^{118}Sn could differ from those in its neighbors. We begin by noting the configurations that are likely to be prominent at the Fermi surface in ^{116}Sn through ^{124}Sn and then calculate $g(2_1^+)$ values in a limited basis shell model with effective values for the nucleon *g* factors in the M1 operator.

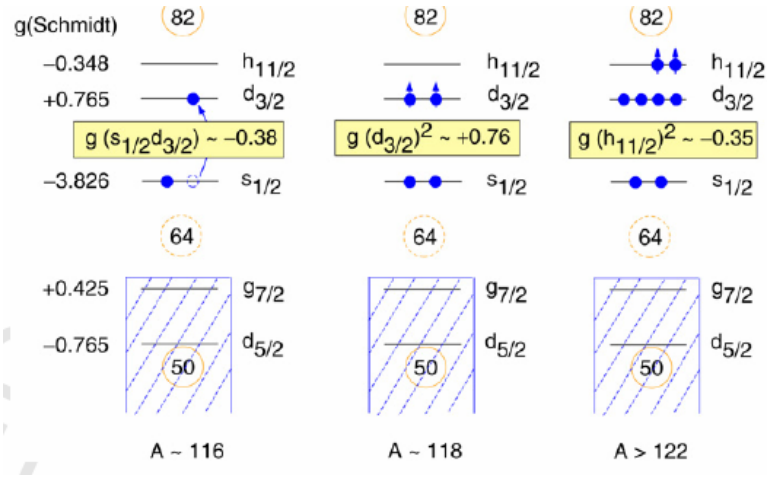

Fig. 2. Single-neutron orbits and *g* factors of configurations near the Fermi surface in $^{116–124}$Sn.

Fig. 2 gives a schematic picture of the configurations near the Fermi surface around ^{118}Sn and their diagonal contributions to the *M*1 operator. This picture attributes some magicity to ^{114}Sn ($N = 64$) and assigns the single-particle order from the spectrum of ^{115}Sn. For ^{116}Sn, the most energetically favorable configuration for a 2^+ state is likely to be $(s_{1/2}d_{3/2})_{2+}$, with a Schmidt (bare nucleon) *g* factor of -0.38. With four 'valence' neutrons in ^{118}Sn, the $s_{1/2}$ orbital is filled and the $(d^2_{3/2})_{2^+}$ configuration, with $g = +0.76$, may be prominent. In this simplified picture, once the $d_{3/2}$ orbit is filled beyond ^{120}Sn, the $(h^2_{11/2})_{2^+}$ configuration with $g = -0.35$ can be expected to become dominant.

To make a more quantitative interpretation, the *g* factors of $^{116–124}$Sn were compared with shell model calculations, performed with OXBASH [22]. These calculations took a similar approach to those reported by Jakob et al. [15] for the Te and Xe isotopes near $N = 82$. Here, however, the basis space assumed a ^{114}Sn core and three valence neutron orbitals, $2s_{1/2}$, $1d_{5/2}$ and $0h_{11/2}$. The singleparticle energies were taken from the experimental levels in ^{115}Sn. Neutron-neutron interactions were calculated with a surface delta interaction of strength, $Avv = 0.21$ MeV, adjusted to reproduce the excitation energies of the low-excitation states in ^{116}Sn. Magnetic moments were then calculated taking $g_s = -2.0$ and $g_l = 0.2$, values chosen to reproduce the *g* factors of the lowest $1/2^+$ and $11/2^-$ states in ^{115}Sn. Holt et al. [5] have also performed shell model calculations in a similar basis for $^{120–130}$Sn, but with more sophisticated interactions. Unfortunately they did not report *g* factors.

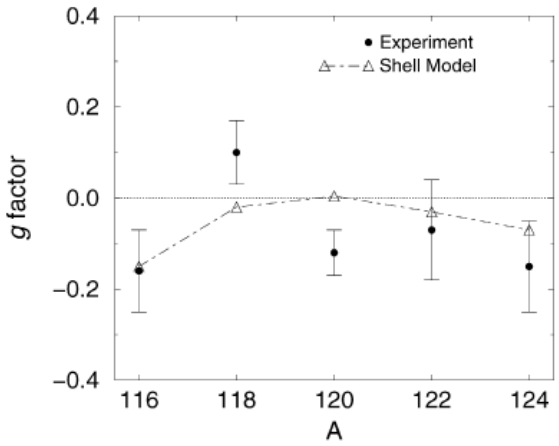

Fig. 3. Adopted *g* factors of 2^+_1 states in Sn isotopes compared to shell model calculations.

Results of the present shell model calculations are shown in Fig. 3. The calculated $g(2^+_1)$ value for ^{116}Sn agrees well with the experimental value. For the heavier isotopes, the calculation reproduces the qualitative trend of an increase and then a gradual decline in $g(2^+_1)$. The calculated *g* factors are evidently very sensitive to configuration mixing, which is determined by the residual interactions and the effective ordering of the neutron orbits at the Fermi surface, as is the level ordering in the odd-*A* isotopes. Holt et al. [5] have noted that the orbitals $1d_{3/2}$, $0h_{11/2}$ and $2s_{1/2}$ are "closely degenerate", which makes it difficult to reproduce the correct level ordering in the odd Sn isotopes. In our calculations the order of the three lowest levels in ^{117}Sn is correct ($1/2^+$, $3/2^+$, $11/2^-$), in ^{119}Sn the order of the $1/2^+$ and $3/2^+$ levels is reversed compared to experiment, and in ^{121}Sn the theoretical order is the opposite of experiment ($3/2^+$, $11/2^-$, $1/2^+$). Improved interactions and/or single-particle energies, possibly dependent on mass [4], might better reproduce the odd-*A* level order and locate the more positive *g* factor at $A = 118$.

We conclude that the limited-basis shell model calculations are in satisfactory agreement with experiment and that the observed $g(2^+_1)$ value in ^{118}Sn is most likely associated with the presence of the $d_{3/2}$ orbital near the Fermi surface.

2. Magnitude of the *g* factors in the Sn isotopes

Turning to the question of the overall magnitude of the *g* factors across the range of isotopes from ^{116}Sn to ^{124}Sn, there is a considerable range in the theoretical predictions. For example, an older calculation by Lombard [2], using a simple random phase approximation (RPA) model with Quadrupole-Plus-Pairing interactions, predicts a monotonic

decrease in $g(2_1^+)$ from +0.16 at ^{112}Sn to -0.076 for ^{124}Sn, in reasonable agreement with the signs and magnitudes of the experimental *g* factors. More recent QRPA [6] and RQRPA [11] calculations are compared with experiment in Fig. 4. The QRPA calculations by Teriyaki et al. [6] for $^{116-124}$Sn are in overall agreement with experiment, predicting *g* factors of about -0.06 for all of these isotopes. In contrast, the recent RQRPA calculations of Ansari and Ring [11] predict a monotonic decrease in $g(2_1^+)$ values from ~+0.25 at A = 112 to ~ +0.1 at A = 124; the magnitude and sign of these theoretical *g* factors does not agree with experiment, except perhaps for the case of 118Sn.

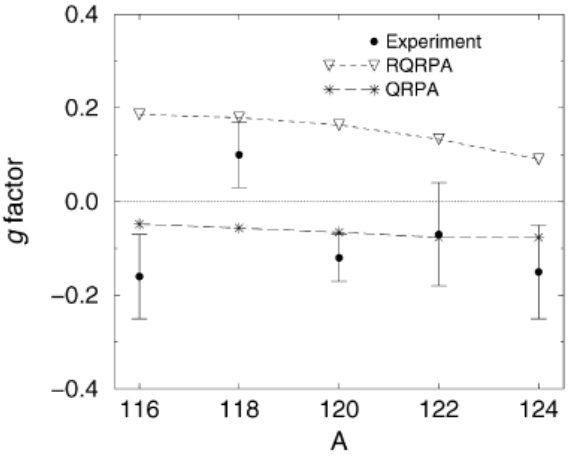

Fig. 4. Comparison of QRPA [6] and RQRPA [11] calculations with the experimental *g* factors of 2_1^+ states in Sn isotopes.

The difference between the *g* factor predictions for these two models appears to stem from the fact that the RQRPA calculation has a proton contribution to the total wavefunction normalization, I_p, approaching 10 % whereas the QRPA calculation has I_p nearer to 5 % (see Fig. 2 in Ref. [11] and Fig. 13 in Ref. [6].) Because the *g* factors are extremely sensitive to the proton content of the wavefunction, a difference between the proton contributions of the order of 5 % leads to a very large difference in predicted *g* factors. It is evident from Fig. 3 of Ref. [11], that the positive theoretical *g* factors in the RQRPA calculation originate from the proton orbital contribution and are not substantially affected by the choice for the orbital and spin *g* factors, which are somewhat different in the QRPA calculation [6].

The above discussion has emphasized that the *g* factors of the Sn isotopes are extremely sensitive to the proton content of the wavefunction. Recent *B*(E2) measurements in combination with large basis shell model calculations have concluded that there must be proton particle-hole excitations across Z = 50 in these isotopes [7, 8]. Although performed for a different purpose, the results of the present limited basis shell model (which do not include proton excitations) are not inconsistent with this conclusion. In particular, the overall magnitude of the *g* factors in the present calculations is determined largely by the effective g_l and g_s values adopted for the neutrons, which differ significantly from the unquenched (bare-nucleon) values. In fact, our adopted value for the anomalous orbital magnetism of the neutron, δg_l = +0.2, is considerably more positive than the value expected from meson exchange, $\delta g \approx$ -0.03 [23]. A shell model description with bare g_l and g_s would evidently require a proton component in the wavefunction. To investigate this aspect further, the $g(2^+)$ values in our limited-basis shell model calculation were re-evaluated with the bare nucleon *g* factors. In all cases the outcome was a shift by about -0.15 from the values shown in Fig. 3. An orbital proton contribution of the order of 6% would be needed to cancel this offset. Whatever the relative contributions from orbital and spin angular momentum, it is clear that the present experimental results strongly constrain the proton content of the 2^+ wavefunctions in the Sn isotopes. A quantitative comparison of the experimental *g* factors with the large basis shell model calculations that account for the *B*(E2) data is needed.

As a final comment, the present results show that *g* factors can be very sensitive to the single-particle structure near the Fermi surface. Indeed the sensitivity can be such that *g*-factor measurements on exotic nuclei (where new shell structure is proposed) could prove extremely useful, even in cases where the experimental precision is limited.

Acknowledgement

The authors are grateful to the academic and technical staff of the Department of Nuclear Physics (Australian National University) for their support. This work was supported in part by the Australian Research Council Discovery Scheme, grant No. DP0773273.

REFERENCES

1. *Kisslinger L.S., Sorensen R.A.* // Rev. Mod. Phys. - 1963. - Vol. 35. - P. 853.
2. *Lombard R.J.* // Nucl. Phys. - 1968. - Vol. A 114. - P. 449.
3. *Hass M., Broude C., Niv Y., Zemel A.* // Phys. Rev. - 1980. - Vol. C 22. - P. 97.
4. *Andreozzi F. et al.* // Z. Phys. - 1996. - Vol. A 354. - P. 253.
5. *Holt A., Engeland T., Hjorth-Jensen M., Osnes E.* // Nucl. Phys. - 1998. - Vol. A 634. - P. 41.
6. *Terasaki J., Engel J., Nazarewicz W., Stoitsov M.* // Phys. Rev. - 2002. - Vol. C 66. - P. 054313.
7. *Banu A. et al.* // Phys. Rev. - 2005. - Vol. 72. - P. 061305(R).
8. *Cederkll J. et al.* // Phys. Rev. Lett. - 2007. - Vol. 98. - P. 172501.
9. *Vaman C. et al.* // Phys. Rev. Lett. - 2007. - Vol. 99. - P. 162501.
10. *Stone N.J.* // At. Data Nucl. Data Tables. - 2005. - Vol. 90. - P. 75.
11. *Ansari A., Ring P.* // Phys. Lett. - 2007. - Vol. B 649. - P. 128.

12. *Stuchbery A.E., Ryan C.G., Bolotin H.H., Sie S.H.* // Phys. Rev. - 1981. - Vol. C 23. - P. 1618.
13. *Stuchbery A.E. et al.* // Nucl. Phys. - 1985. - Vol. A 435. - P. 635.
14. *Robinson M.P. et al.* // Nucl. Phys. - 1999. - Vol. A 647. - P. 175.
15. *Jakob G. et al.* // Phys. Rev. - 2002. - Vol. C 65. - P. 024316.
16. *Benczer-Koller N., Kumbartzki G.J.* // J. Phys. G: Nucl. Part. Phys. - 2007. - Vol. 34. - P. R321.
17. *Stuchbery A.E. et al.* // Phys. Rev. - 2007. - Vol. C 76. - P. 034306.
18. *Shu N.K.B. et al.* // Phys. Rev. - 1980. - Vol. C 21. - P. 1828.
19. *Ziegler J.F., Biersack J.P., Littmark U.* // The Stopping and Ranges of Ions in Matter. Vol. 1. The Stopping and Range of Ions in Solids / Ed. by J.F. Ziegler. - New York: Permagon, 1985.
20. *Luontama M. et al.* // Z. Phys. - 1986. - Vol. A 324. - P. 317.
21. *Svensson L.E. et al.* // Nucl. Phys. - 1995. - Vol. A 584. - P. 547.
22. *Brown B.A. et al.* Oxbash for Windows PC, Michigan State University, report N. MSU-NSCL 1289, 2004.
23. *Brown B.A. et al.* // Phys. Rev. - 2005. - Vol. C 71. - P. 044317.